Cyclic AMP Regulation of Protein Lysine Acetylation in Mycobacterium Tuberculosis

Published in final edited form as:
Nat Struct Mol Biol. 2012 August ; 19(8): 811–818. doi:10.1038/nsmb.2318.

Cyclic-AMP regulation of protein lysine acetylation in *Mycobacterium tuberculosis*

Ho Jun Lee[1], **P. Therese Lang**[1], **Sarah M. Fortune**[2], **Christopher M. Sassetti**[3], and **Tom Alber**[1]

[1]Department of Molecular and Cell Biology and QB3 Institute, University of California, Berkeley, CA 94720, USA

[2]Department of Immunology and Infectious Diseases, Harvard School of Public Health, Boston, MA 02115, USA

[3]Department of Molecular Genetics and Microbiology and Howard Hughes Medical Institute, University of Massachusetts Medical School, Worcester, MA 01655, USA

Abstract

Protein lysine acetylation networks can regulate central processes such as carbon metabolism and gene expression in bacteria. In *Escherichia coli,* cyclic-AMP (cAMP) regulates protein lysine acetyltransferase (PAT) activity at the transcriptional level, but in *Mycobacterium tuberculosis*, fusion of a cyclic-nucleotide binding domain to a Gcn5-like PAT domain enables direct cAMP control of protein acetylation. Here we describe the allosteric activation mechanism of *M. tuberculosis* PAT. The crystal structures of the auto-inhibited and cAMP-activated PAT reveal that cAMP binds to a cryptic site in the regulatory domain over 32 Å from the catalytic site. An extensive conformational rearrangement relieves auto-inhibition by a substrate-mimicking lid that covers the protein-substrate binding surface. A steric double latch couples the domains by harnessing a classic, cAMP-mediated, conformational switch. The structures suggest general features that enable the evolution of long-range communication between linked domains.

Keywords

evolution of allosteric regulation; Rv0998; domain coupling; conformational change; Ringer

Protein domains have long been recognized as functionally modular [1]. Domain shuffling in exons in eukaryotes, for example, enables rapid duplication and divergence of protein families [2,3]. Recombination produces numerous assortments of domains that mediate hybrid processes [4], and domain fusions signal cooperating activities [5]. Kuriyan and Eisenberg proposed that fusions are a common initial step in the evolution of allosteric regulation [6], but this view of the structural autonomy of domains like beads on a string has turned attention

Address correspondence to: Tom Alber<tom@ucxray.berkeley.edu>, Ph: 510-642-8758, Fax: 510-666-2768.

Accession codes

The coordinates and structure factors were deposited in the Protein Data Bank, under accession numbers 1AVA (auto-inhibited Mt-PatA), 1AVB, and 1AVC (cAMP-activated Mt-PatA).

Contributions

H.J.L. conducted all the biochemical and crystallographic studies. P.T.L. conducted the computational studies with *Ringer*. T.A., H.J.L., P.T.L. and C.M.S. wrote the manuscript. All authors discussed the results and commented on the manuscript.

Competing financial interests

The authors declare no competing financial interests.

away from the problem of how domains evolve to work in concert to enable tight functional regulation [7]. Here we explore the particularly dramatic mechanisms of functional domain interdependence in the cyclic-AMP-regulated protein lysine acetyl transferase (PAT) of *Mycobacterium tuberculosis.*

Reversible protein acetylation is an important regulatory mechanism that controls numerous cellular processes in all three kingdoms of life [8,9]. Proteomic studies in prokaryotes and eukaryotes have detected thousands of lysine-acetylated proteins, a number that rivals phosphoproteins [9]. Protein lysine acetylation controls diverse cellular processes, including chromatin structure, chromosomal segregation, cytoskeletal dynamics, and chaperone function. The emerging role for this modification in controlling mitochondrial metabolism [10,11] highlights the remarkable conservation of this regulatory strategy. Recent discoveries have revealed that protein lysine acetylation globally regulates carbon metabolism in diverse bacterial species [12-14]. Stimuli such as different carbon sources alter acetylation patterns of >100 proteins in *Escherichia coli* and *Salmonella* to change the direction of carbon flux to glycolysis or gluconeogenesis and to control the activity of the glyoxylate shunt relative to the TCA cycle. However, distinct networks couple protein acetylation to growth conditions in prokaryotes [15].

In enteric bacteria, Gcn5-related *N*-acetyltransferase (GNAT) PAT activity is controlled at the transcriptional level [16]. Increases in the concentration of cyclic-AMP (cAMP), a universal second messenger that modulates diverse functions in response to environmental conditions, indirectly mediate this transcriptional stimulation. The cAMP complex of the catabolite activator protein (CAP) induces the expression of genes for pathways required for the utilization of alternative carbon sources or, in the absence of other substrates, restructures central carbon metabolism for slow growth [17]. Indeed, cAMP has been shown to be the dominant regulator controlling carbon fluxes in glucose-limited cultures. The *E. coli patZ* acetyltransferase gene, for example, is activated ~10-fold by entry into stationary phase or growth on acetate compared to growth on glucose [16]. Binding of the CAP-cAMP complex to two sites in the *patZ* promoter mediates this transcriptional activation.

In contrast in *M. tuberculosis*, cAMP directly activates the single Gcn5-like enzyme, Rv0998 [18], which we call Mt-PatA. Cyclic-AMP mediates this allosteric regulation by binding to a cyclic-nucleotide binding domain fused to the N-terminus of the catalytic PAT domain [18]. While the substrates of Mt-PatA have not been globally identified, it has been proposed to inhibit the acetate catabolic enzyme, acetyl-CoA synthetase (ACS) [19]. Although no conditions have been found in which Mt-PatA acetylates purified ACS *in vitro*, the purified *Mycobacterium smegmatis* ortholog (MSMEG_5458) acetylates both *M. smegmatis* and *M. tuberculosis* ACS [19]. The universal stress protein (USP; MSMEG_4207), a homolog of proteins involved in adaptation to growth-limiting conditions [20], is an *in vitro* substrate of both mycobacterial PatA enzymes [18]. *M. tuberculosis* lacks a USP protein, however, making USP a nonphysiological substrate. Nonetheless, *in vitro* USP acetylation has enabled the characterization of Mt-PatA activity and regulation [18]. The *M. tuberculosis* NAD^+-dependent deacetylase, Rv1151c, reverses Mt-PatA modifications and creates a reversible protein acetylation system [18,19].

The biological functions of Mt-PatA in adapting to different carbon sources and shifting to slow growth appear to have been conserved across diverse bacteria [12-14,21], but the allosteric mechanism by which cAMP regulates protein acetylation is specific to mycobacteria. To understand how distinct, functionally independent domains can be fused to enable this unique control strategy, we determined the structures of the auto-inhibited and cAMP-activated states of Mt-PatA. We found that sequences inserted in the PAT domain simultaneously regulate the accessibility of the regulatory and catalytic sites. This switch

harnesses a dramatic conformational transition in the cAMP regulatory module to control the exposure of the catalytic site over 32 Å away in the structures. The Mt-PatA structures afford unanticipated insights into the functional requirements of the evolutionary steps following domain fusion that amplify emergent allosteric regulation.

RESULTS

Structure of Mt-PatA

The Mt-PatA sequence contains an N-terminal cNMP-binding domain (residues 12-142) fused to a GNAT-family catalytic domain (residues 146-314) followed by a C-terminal extension (residues 315-333). To determine how the regulatory and catalytic domains are linked together to enable cAMP to control catalytic activity, we determined the crystal structures of the auto-inhibited and active forms of the enzyme (Table 1). Despite the absence of acetyl-CoA in the crystallization conditions, the structures contained this substrate carried through the purification from intracellular pools. We determined the structure of the active cAMP complex in two crystal forms at 1.8- and 2.8-Å resolution. Because the structures of monomers derived from different space groups are similar (root-mean-square deviation (rmsd) = 0.70 Å for all 327 Cα atoms), the higher resolution structure was used to represent the active conformation.

The 1.7-Å-resolution structure of Mt-PatA in the absence of cAMP (Fig. 1a) reveals that at least two mechanisms autoinhibit the enzyme. The first domain adopts the fold of a typical cAMP-binding regulatory module (Supplementary Fig. 1a), but remarkably, the C-terminus of the protein occupies the cAMP-binding site, excluding the ligand (Fig. 1b). The C-terminal extension forms a helix that is just long enough to project the terminal carboxylate into the cryptic activator site, where it structurally mimics a bound cyclic phosphate group. A short extended loop (residues 143-145) packed against the C-terminal helix tightly links the two functional domains. The PAT domain shows structural homology to the GNAT family (Supplementary Fig. 1c). Acetyl-CoA binds in a shallow cleft formed by structurally conserved motifs [22] (Fig. 1c). Unexpectedly, a large loop (residues 161-203) integrated into the catalytic domain forms a lid that folds over the catalytic site and excludes protein substrates (Fig. 1a). His173 in the lid engages the predicted catalytic base, Glu235, and the activated acetyl group, analogous to a lysine substrate (Fig. 1d). Thus, the C-terminal helix and the lid represent dedicated regulatory elements of the PAT domain that form a steric double latch that limits enzyme activity. The regulatory and catalytic sites are separated by over 32 Å, raising the question of the mechanism of long-range communication between the domains.

Structure of the active Mt-PatA:cAMP:Ac-CoA complex

Dramatic conformational changes accompany cAMP binding to the regulatory domain (Fig. 2). A difference-distance matrix reveals relative structural shifts of up to 40 Å (Fig. 2a). The regulatory domain pivots ~40° around Ser144 in the interdomain linker, resulting in a strikingly different orientation with respect to the catalytic domain (Fig. 2b). This rotation removes the C-terminus from the cAMP binding site. In the cAMP-activated Mt-PatA, the 44-residue lid refolds, exposing the catalytic site, further burying the Ac-CoA substrate and revealing a conserved surface adjacent to the substrate-binding site (Fig. 2c).

Tertiary changes in regulatory domain stabilized by cAMP are coupled to release of the lid from the PAT active site. While the topology of the regulatory domain is retained in the auto-inhibited and active forms (rmsd = 2.76 Å for all 134 Cα atoms), the β-sheet is the rigid element in the structure (Cα rmsd = 0.85 Å for residues 37-113; Fig. 3a). The α-helices that start and end the domain shift and undergo tertiary structural changes

(Supplementary Fig. 2a). Rotating around Gly113, helices C (residues 26-35), E (residues 115-123) and F (residues 127-142) move >10 Å relative to the sheet to enable Arg138 and Phe142 to sandwich the adenine ring against Val67 in the sheet (Figs. 3a, 3b). This altered conformation of helix F completes the cAMP binding site.

To define the side-chain shifts that enable these large structural changes, we systematically compared the rotamer distributions in the auto-inhibited and cAMP-activated structures using the program *Ringer* [23]. *Ringer* automatically samples the electron density map around each side-chain dihedral angle, and the correlation coefficients (ccs) of *Ringer* plots can highlight changes in rotamer ensembles even when the underlying models are similar [23,24]. While distributions with ccs <0.5 often differ the major populated rotamer, a conservative cc threshold of 0.2 was used to automatically define sites that switch rotamers between the two structures (Supplementary Figs. 2b, 2c). In typical control structures in the PDB where changes in crystal packing are the only perturbations, very few residues give *Ringer* correlation coefficients <0.2 (Supplementary Figs. 2d, 2e). In contrast, Mt-PatA, activation is associated with extensive remodeling of side-chain distributions (Figs. 3c and 3d; Supplementary Fig. 2c). Residues in helices A, B, C and E, as well as the underlying β-sheet of the regulatory domain, adopt new rotamers upon cAMP binding (Fig. 3c). The refolding of the lid remodels rotamers on the surface of the protein from helix E all the way to the active site (Fig. 3d; Supplementary Fig. 2c). The newly exposed, conserved surface (Fig. 2c) near the acetyl donor populates many new rotamers. The core of the PAT domain and most of the C-terminal helix, in contrast, retain similar structures upon activation.

Communication between the regulatory and catalytic domains

Comparison of the structures reveals that the regulatory and catalytic domains communicate with each other by forming sterically incompatible conformations in the active and auto-inhibited states. In the auto-inhibited state, helix F of the regulatory domain is nearly parallel to helix I (residues 193-202) of the lid domain. However, helix F reorients in the active conformation due to the rotation of the regulatory domain, which requires a movement of the lid to avoid steric clashes between these helices (Fig. 3e). The lid domain refolds into a distinct backbone arrangement (Supplementary Fig. 3a). Many lid residues move >15 Å, and helix I rotates toward the catalytic domain by 65° (Fig. 3e). Cyclic AMP favors the “open” state of the two steric latches by stabilizing a rotation of the regulatory domain that creates the activator binding site and simultaneously generates a steric clash with the inhibitory structure of the lid. Refolding of the lid enables the rotation of the regulatory domain that creates the cAMP binding site.

The comparison of active and auto-inhibited structures suggests that activation by cAMP stabilizes the open lid. To test this two-state coupling model, we took advantage of the mimicry of a bound substrate by His173 in the auto-inhibited conformation. The lack of conservation of this residue in the closely related *M. smegmatis* ortholog suggests that its main role is to block substrate access in the absence of cAMP. The His173Lys substitution introduced the only Lys in the sequence. Consistent with the close approach of His173 to the acetyl donor (Fig. 1d), we found that the His173Lys mutant readily auto-acetylated the new lysine in the absence of cAMP (Fig. 4a). Addition of cAMP blocked this auto-acetylation, consistent with the structure of the active state in which His173 in the open lid is 25 Å away from the acetyl donor (Supplementary Fig. 3b). In contrast, cAMP stimulated acetylation of *M. smegmatis* USP by the His173Lys variant (Fig. 4b), indicating that the mutation did not alter the normal regulation of the enzyme.

A two-state model further predicts that the auto-inhibited structure stabilizes the closed conformation of the lid in which the acetyl-Lys173 is buried, while cAMP stabilizes active form in which residue 173 is fully solvent exposed. To test the accessibility of acetyl-

Lys173, we measured the activity of the deacetylase, Rv1151c, in the presence and absence of cAMP. Under conditions in which the auto-acetylated Mt-PatA His173Lys was fully deacetylated in <10 min in the presence of cAMP, the auto-inhibited form protected acetyl-Lys173 for >2 hours (Fig. 4c). In contrast, cAMP does not affect the deacetylation of a control substrate, *M. smegmatis* USP (Fig. 4c). These results suggest that the lid is not simply a flexible element, but rather that it forms alternate structures in the presence and absence of cAMP in agreement with the distinct arrangements observed in the crystal structures of the active and auto-inhibited states (Figs. 2b, 3e; Supplementary Fig. 3).

To investigate the role of the C-terminal helix in forming a steric latch, we changed the length of the protein by adding or subtracting residues. Interestingly, deleting the last four residues, which removes the C-terminus from the cAMP binding site, preserved activity and activation by cAMP, but imparted low acetyl-transfer activity even in the absence of the activator (Fig. 4d). Strikingly, compared to the −4 deletion, addition of one residue (Ser or Arg) at the C-terminus activated the protein more strongly in the absence of cAMP. The deletion of four residues or addition of a single residue also accelerated deacetylation of His173Lys variants (Supplementary Fig. 4), suggesting that these mutations preferentially destabilize the auto-inhibited conformation. In contrast, deletions of up to three residues that maintain important contacts in the auto-inhibited structure (including the polar network formed by Asp73, Arg326 and Glu330 (Supplementary Fig. 4h)) preserved the auto-inhibition and the deacetylation pattern. Moreover, non-physiological high concentrations of cGMP and cCMP also activated the enzyme (Supplementary Fig. 5a), and mutations of conserved residues in the cAMP binding site blocked activation (Fig. 4e). These results implicate the C-terminal steric latch in the switch in the conformation of helix F and the rotation of the regulatory domain in activating the enzyme. The activation by C-terminal insertions or deletions suggests that cAMP stabilizes an intrinsic active population, rather than inducing a specific new structure.

Activity of the PAT domain

The central catalytic core of the PAT domain is structurally homologous to other GNAT-family proteins (Supplementary Fig. 1c). In the active conformation, the open lid forms a conserved surface adjacent to the substrate-binding site (Fig. 2c) that creates a narrow tunnel that allows the substrate Lys side chain to access to the acetyl donor (Fig. 5a). The entrance to the cavity is surrounded by Glu235, the conserved catalytic base, Arg184, which is positioned to reduce the pK_a of the substrate Lys, and the hydrophobic surfaces of side chains (e.g. Phe185, Arg223, Val225, and Ala237), that can complement the aliphatic tail of the Lys acceptor (Fig. 5b). Arg184 is particularly interesting, as it is buried under the lid and Phe185, and it forms a hydrogen bond to the adjacent Arg223 at the bottom of a water-filled tunnel on the backside of the lid (Figs. 5a, 5b). Upon activation, lid residues Arg184 and Phe185 shift >25 Å (Supplementary Figs. 3b, 3c).

Mutational analysis emphasizes the importance of these residues for catalyzing acetyl transfer. The Glu235Ala mutation abolished detectable transfer activity and mutations of residues potentially involved in the complementary interaction with the aliphatic tail of the substrate Lys significantly decreased (Arg223Ala, Val225Ala) or completely abolished activity (Arg184Ala, Phe185Ala, Ala237Val) (Figs. 4e, 5c). The Arg223Ala variant showed significantly reduced activity with an altered pH-rate profile (Fig. 5c). The Arg223Ala mutation abolishes the direct interactions with Arg184, consistent with a dual role for this network of residues in providing the binding site for the substrate and lowering the pKa of the Lys-ε-amino-group nucleophile.

The presence of a cavity beyond the acetyl donor led us to measure the relative activities with different substrates (acetyl-CoA, propionyl-CoA, and butyryl-CoA) on USP, a

heterologous, noncognate protein substrate (Supplementary Fig. 5b-d). The addition of an excess of an equimolar mixture of the three CoA donors resulted in 1.0:1.6:1.3 ratio of acetyl-:propionyl-:butyryl-USP (Supplementary Fig. 5e). These results suggest Mt-PatA can efficiently turn over alternative acyl donors. Accordingly, it may be fruitful to characterize the distributions and functions of these alternative modifications in cells. As acetylation and propionylation have been shown to regulate pathways necessary for the assimilation of acetate and propionate, respectively[19,25], it will be of interest to determine if these modifications have distinct effects on target enzymes.

DISCUSSION

In this work, we have defined the unique mechanism by which mycobacteria couple cAMP concentration to protein lysine acetylation. Our structural and biochemical analysis defines two distinct functional states of the acetyltransferase, Mt-PatA. Dramatic structural changes required for cAMP binding are coupled to exposure of the catalytic site. In the auto-inhibited state, cAMP-binding site is blocked by the C-terminal helix from the catalytic domain. In addition, the substrate-mimicking lid in the catalytic domain buries the acetyl donor and a conserved surface that forms the protein-substrate-binding site. While excluding the C-terminus, cAMP stabilizes the rotation of the regulatory domain as well as tertiary shifts that are incompatible with the closed lid. These shifts release the steric double latch created by the lid and the C-terminal extension of the PAT domain (Fig. 6). The lid rearranges in the active state, creating a large binding surface for protein substrates.

Our results disfavor a sequential model in which cAMP binding initiates a specific mechanical pathway for the conformational change. Importantly, there is no site for cAMP to bind before the enzyme switches conformations (Fig. 1), and once cAMP stabilizes the active form, the lid does not readily fluctuate back to the inhibited conformation (Figs. 2, 3, 4; Supplementary Figs. 3, 4). In addition, C-terminal mutations designed to destabilize the latch at the regulatory site activate the enzyme in the absence of cAMP (Fig. 4d). This gain of function shows that cAMP is not needed to induce the active conformation in the mutants. These findings support a two-state model for activation mediated by steric incompatibility of the alternate conformations. In this model, the relative stability of the two globally different conformations mediates the communication between the regulatory and catalytic sites. Consistent with changes in hydrogen exchange in peptides throughout the protein upon cAMP binding [26], the widespread changes in rotamers detected using *Ringer* and the effects of diverse mutations on activation provide evidence that changes in interactions all over the enzyme determine the relative stability of the two states.

Diverse proteins containing a cAMP-binding module--including CAP, hyperpolarization-activated cyclic nucleotide-modulated (HCN) channels, and the regulatory subunit of protein kinase A--have been structurally characterized. Although these proteins mediate different biological functions, they all contain a conserved module for cAMP binding that allosterically controls activity [27,28]. The cAMP-binding modules have similar architectures, but show significant structural variations in the helical subdomain and the loop between strands 4 and 5 (using Mt-PatA numbering; Supplementary Fig. 2). The core β-subdomain is structurally similar (rmsd = 0.73-1.00 Å for ~70 Cα atoms of Mt-PatA (Supplementary Fig. 1a), and the key residues that interact with cAMP also are conserved among cAMP-binding modules (Supplementary Fig. 1b).

Cyclic-AMP binding to Mt-PatA requires a >10 Å movement of helix F (residues 127-142) in the regulatory domain. Similarly in *E. coli* CAP [28-30], cAMP stabilizes a restructuring in the helix bearing cAMP-binding residues, linked to a coil-to-helix transition with many residues moving >10 Å (Supplementary Figs. 6a-c). These changes result in steric clashes

that are resolved by flipping out the CAP DNA-binding domains. The solution structure of apo-CAP determined using NMR shows that the cAMP binding site is not present in the major conformer in the absence of activator [28]. Like the cryptic cAMP site of Mt-PatA, this suggests that the conformation switches before the nucleotide binds. Moreover, NMR measurements demonstrate that two constitutively activating CAP mutations switch the population toward the active conformation in the absence of activator [28], as embodied in the design of C-terminal mutants of Mt-PatA (Fig. 4d). In contrast, the cAMP binding site is better formed in the crystal structure of apo-CAP, and the crystallographic results have been interpreted in terms of a sequential activation model [30]. Nonetheless, genetic, biochemical and NMR studies of *E. coli* CAP [28] indicate that the two-state model for Mt-PatA activation captures general features of cAMP-regulated systems.

Large structural shifts also occur in the RIα inhibitory subunit of human cAMP-dependent protein kinase, where cAMP binding stabilizes dramatic conformational changes through the connecting helix (αB/C) that release the regulatory subunit [31]. These examples emphasize the general role of the cAMP binding domain in regulating large conformational changes, not subtle shifts [32]. By modulating the position of the helical subdomain, cAMP binding favors significant structural changes that must be accommodated in the attached functional domains by changes that are commensurate in magnitude [32]. While cAMP mediates large shifts, the structural responses in regulated domains are distinct in different systems (Supplementary Figs. 6d-g).

The selective pressures that shaped the evolution of cAMP regulation of Mt-PatA remain to be defined. Bacterial pathogens including *M. tuberculosis* commonly utilize cAMP as an important regulator of gene expression and host signaling to promote survival in changing environmental conditions [15,33]. The cellular dynamics of cAMP are determined by the interplay of synthetic adenylyl cyclases (ACs) and hydrolytic cyclic nucleotide phosphodiesterases (PDEs). The *M. tuberculosis* genome encodes 10 predicted cAMP-binding proteins, one PDE, as well as an unusually large number of ACs (15 and 17 in strains H37Rv and CDC1551, respectively) [34].

In contrast, other bacterial pathogens such as *E. coli* and *Pseudomonas* have only one AC gene. This expansion of AC sequences suggests that Mt-PatA forms the nexus of multiple signaling pathways that modulate cAMP levels. While the CAP transcription-factor family mediates many of the effects of cAMP, the cAMP-signaling cascade in mycobacteria is remodeled to mediate direct post-translational regulation of protein lysine acetylation without the requirement for new gene expression [18]. *M. tuberculosis* is thought to persist in a relatively quiescent state during infection [35,36], and dormant mycobacteria may produce little new mRNA or protein [37]. Moreover, rapid changes in metabolism may be required to tolerate host immune defenses. Thus, the structure of the Mt-PatA we describe may be specialized to allow rapid regulation under growth-limiting conditions. The conservation of the residues that contact cAMP (Supplementary Fig. 1b), however, may hamper efforts to develop selective inhibitors that target this site in Mt-PatA in preference to human cAMP-binding domains. Rather, control of the Mt-PatA latching mechanisms by stabilizing the auto-inhibited form may afford a more promising strategy for therapeutic development.

While the evolutionary pathway cannot be appreciated experimentally, structural comparisons afford clues to the molecular features that can enable the emergence of this allosteric control. In Mt-PatA, two sequence elements in the catalytic domain and the three-residue linker between the domains harness the conformational switch in the cAMP regulatory module. The lid and the C-terminal helix inserted in the PAT domain do not make direct contacts, but instead interact indirectly through the cAMP-binding module. No regulation is possible without the lid, so this was likely the first regulatory element to be

incorporated. The archaeal PAT from *Sulfolobus solfataricus* provides an example of an isolated PAT domain with an auto-inhibitory lid [38]. Without a regulatory domain, the lid in this archaeal PAT may respond directly to growth conditions. Consistent with the Kuriyan and Eisenberg model [6], fusion of the cAMP binding domain in Mt-PatA and the evolution of interdomain interactions with the lid in the unbound form would provide an evolutionary pathway for metabolites to regulate auto-inhibition. The effects of C-terminal mutations in Mt-PatA show that the addition of the C-terminal helix provides a latch that stabilizes the auto-inhibited form relative to the active form, effectively increasing the cAMP concentration needed for activation. The interdomain linker tightly tethers the domains, preventing the regulatory and PAT domains from diffusing apart. This short covalent linkage restricts the relative motions of the domains to a rotation that functions to reveal cooperatively the cAMP binding site and the active site. This cooperativity of sterically incompatible conformations creates a two-state mechanism of long-range communication that couples regulatory and catalytic sites separated by over 32 Å. Overall, this switch in Mt-PatA affords insights into the structural features that can be exploited in the evolution of allosteric regulation through domain fusion.

Online Methods

Cloning of Mt-PatA and Rv1151c deacetylase from *M. tuberculosis*

The *Rv0998* gene (GenBank™ accession number: CAB08156.1) was amplified by PCR from the genomic DNA of *Mycobacterium tuberculosis* H37Rv using *PfuTurbo* DNA polymerase (Stratagene), introducing unique BamHI and XhoI restriction sites at the N- and C-termini, respectively. Amplified, digested PCR products were ligated into the predigested pGEX-6P-3 vector (GE Healthcare), resulting in an N-terminal, cleavable, Glutathione-S-transferase (GST) tag followed by the Mt-PatA coding sequence. Clones were verified by DNA sequencing (Elim Biopharm).

Indel mutants of Mt-PatA were generated by PCR using the cloned wild-type Mt-PatA construct as a template. Point mutations were generated using the QuikChange method (Stratagene).

Cloning of universal stress protein MSMEG_4207 from *M. smegmatis*

The *msmeg_4207* gene (GenBank™ accession number: ABK72172.1) was amplified from the genomic DNA of *Mycobacterium smegmatis* MC^2 155 by similar procedures described above and cloned into the pGEX-6P-3 vector to introduce a cleavable N-terminal GST tag. Clones were verified by DNA sequencing.

Protein expression and purification

Mt-PatA variants were expressed in BL21-CodonPlus™ (Stratagene) cells induced with 0.1 mM isopropyl β-D-thiogalactopyranoside (IPTG) and grown overnight at 22 °C. Cells were harvested by centrifugation, resuspended in 20 mM Tris-HCl, pH 7.5, 100 mM NaCl with protease inhibitors, lysed by sonication, and the cleared lysate was purified on a GSTrap™ HP column (GE Healthcare). Mt-PatA-GST fractions were cleaved with PreScission Protease (GE Healthcare), reloaded onto the GSTrap™ HP column, and the flow-through fractions were concentrated and purified by gel filtration on a Superdex™ 75 (GE Healthcare) column. Selenomethionine-labeled Mt-PatA was expressed as described [39] and purified in the presence of 1 mM tris(2-carboxyethyl)phosphine (TCEP).

M. smegmatis USP was expressed in BL21-CodonPlus *E. coli* cells induced with 0.5 mM IPTG at 22 °C and purified as described above for Mt-PatA. His-tagged Rv1151c deacetylase was expressed similarly, and harvested cells were resuspended in 20 mM

HEPES, pH 7.5, 500 mM NaCl, 25 mM imidazole and lysed by sonication. The cleared lysate was purified on a Ni- charged HiTrap Chelating HP column (GE Healthcare) using a 25-300 mM imidazole gradient. The protein was concentrated and purified by gel filtration on a Superdex™ 75 column in 20 mM Tris-HCl, pH 7.5, 100 mM NaCl.

In vitro protein acetylation and deacetylation assays

Acetylation assays were carried out in 20 mM buffer, 100 mM NaCl, 100 μM acetyl-CoA, 20 μM USP in the presence and absence of 200 μM cAMP. Reactions were initiated by the addition of 20 μM Mt-PatA, incubated for 10 min at 22 °C, and quenched by boiling in SDS loading dye. Buffers were as follows: sodium acetate (pH 4.0-5.0), MES (pH 6.0), HEPES (pH 7.0), Tris (pH 7.5-8.0), BisTrisPropane (pH 9.0), and Glycine (pH 10.0). Reactions were analyzed in parallel with SDS-PAGE and Western blotting with anti-AcLys antibody (Cell Signaling Technology) detected quantitatively by chemiluminescence (LI-COR Biosciences).

Deacetylation assays (20 μl) were carried out at 22 °C in 20 mM Tris-HCl, pH 7.5, 100 mM NaCl, 1 mM β-Nicotinamide adenine dinucleotide (NAD^+), 20 μM auto-acetylated Mt-PatA H173K mutant in the presence and absence of 200 μM cAMP. Reactions were initiated by addition of 5 μM Rv1151c and terminated at various time points by boiling in SDS loading dye. Samples were analyzed in parallel using SDS-PAGE and Western blotting using SDS-PAGE and Western blotting with anti-Ac-Lys antibodies.

His173Lys Mt-PatA auto-acetylation

The purified H173K Mt-PatA auto-acetylated *in vivo* was deacetylated twice sequentially using Rv1151c deacetylase in 20 mM Tris-HCl, pH 7.5, 100 mM NaCl, 1 mM NAD^+, 10 μM Mt-PatA H173K, 200 μM cAMP and 5 μM His-tagged Rv1151c. The deacetylation reaction was initiated by the addition of His-tagged Rv1151c to the reaction mixture and incubated at 22 °C for 2 h. The reaction mixture was loaded onto a Ni-charged HiTrap column and flow-through fractions were collected, followed by dialysis against 20 mM Tris-HCl, pH 7.5, 100 mM NaCl overnight at 4 °C. Dialyzed protein was subjected to the second deacetylation step using identical procedures to remove residual acetyl-Lys formed during the dialysis due to the bound acetyl coenzyme-A carried over from cells in the course of expression. The double-deacetylated H173K mutant was assayed for reacetylation in 20 mM Tris-HCl, pH 7.5, 100 mM NaCl, 10 μM Mt- PatA H173K, 100 μM Ac-CoA in the presence and absence of 200 μM cAMP. Samples were analyzed using SDS-PAGE and Western blotting.

Comparison of activity with different CoA donors

Assays were carried out in 20 mM Tris-HCl, pH 7.5, 100 mM NaCl, 1 μM Mt-PatA, 200 μM cAMP, 1 mM CoA donor(s) (Acetyl-, Propionyl-, and Butyryl-CoA), 100 μM *M. smegmatis* USP. Masses of reaction products were determined using Liquid Chromatography Mass Spectrometry (LC/MS).

Crystallization, structure determination and refinement

Mt-PatA:Ac-CoA was crystallized by vapor diffusion from 100 mM sodium cacodylate, pH 6.0, 200 mM magnesium acetate, 20% (w/v) PEG 8K. Two crystal forms of Mt-PatA:Ac-CoA:cAMP were grown by vapor diffusion from 100 mM sodium citrate, pH 5.0, 5 mM cAMP 12% (v/v) isopropanol, and 15% (w/v) PEG 10K. The crystals were transferred into mother liquors containing 25% (v/v) ethylene glycol, and diffraction data were collected at 100 K. X-ray data were processed and scaled using HKL2000 [40] or Mosflm [41] followed by Scala [42].

The structures of auto-inhibited and cAMP-activated Mt-PatA were solved using multi-wavelength anomalous dispersion (MAD) phasing using Phenix AutoSol [43]. Initial models built by Phenix AutoBuild [43] were improved using ARP/wARP [44] and Coot [45]. A model of one molecule of the cAMP-bound form of Mt-PatA was used to place a second molecule in the asymmetric unit using Phaser [46]. Rigid body refinement [47] and automated modeling with Buccaneer [48] were followed by additional cycles of manual model building and refinement [43,47]. The 1.8-Å-resolution cAMP-bound structure was determined using molecular replacement [46] and refined using Phenix Refine [43] with exclusion of 5% of the reflections to calculate R_{free}. Translation/Libration/Screw (TLS) refinement was incorporated at the end of the process. The molecules were packed similarly in the two crystal forms of the activated enzyme.

Ringer correlation coefficients between electron-density maps of the active and auto-inhibited structures were calculated as described [23,24]. Models were validated using Molprobity [49], showing 97.2-98.5% of all ϕ and ψ geometries are in the most favored region, with no outlier in the Ramachandran statistics. Sequence conservation was mapped onto the structures using ConSurf (http://consurf.tau.ac.il). The Pfam database (http://pfam.sanger.ac.uk/) was used to identify functional domains and related sequences. Multiple sequence alignment was performed using ClustalW2 [50]. Secondary structures were assigned using DSSP (Dictionary of Protein Secondary Structure) [51], and structural figures were generated using PyMOL (http://www.pymol.org/) and Chimera [52].

Supplementary Material

Refer to Web version on PubMed Central for supplementary material.

Acknowledgments

We are grateful to James Holton, George Meigs, and Jane Tanamachi at Beamline 8.3.1 at Lawrence Berkeley National Laboratory for help with X-ray data collection. We appreciate the support of the TB Structural Genomics Consortium. This work was supported by a post-doctoral research fellowship from the Canadian Institutes of Health Research to H.J.L. and NIH grants R01GM70962 and P01AI068135 to T.A.

References

1. Frankel AD, Kim PS. Modular structure of transcription factors: implications for gene regulation. Cell. 1991; 65:717–719. [PubMed: 2040012]
2. Dorit RL, Gilbert W. The limited universe of exons. Curr. Opin. Genet. Dev. 1991; 1:464–469. [PubMed: 1822278]
3. Long M, de Souza SJ, Gilbert W. Evolution of the intron-exon structure of eukaryotic genes. Curr. Opin. Genet. Dev. 1995; 5:774–778. [PubMed: 8745076]
4. Geer LY, Domrachev M, Lipman DJ, Bryant SH. CDART: protein homology by domain architecture. Genome Res. 2002; 12:1619–1623. [PubMed: 12368255]
5. Marcotte EM, Pellegrini M, Thompson MJ, Yeates TO, Eisenberg D. A combined algorithm for genome-wide prediction of protein function. Nature. 1999; 402:83–86. [PubMed: 10573421]
6. Kuriyan J, Eisenberg D. The origin of protein interactions and allostery in colocalization. Nature. 2007; 450:983–990. [PubMed: 18075577]
7. Kuriyan J, Cowburn D. Modular peptide recognition domains in eukaryotic signaling. Annu. Rev. Biophys. Biomol. Struct. 1997; 26:259–288. [PubMed: 9241420]
8. Hu LI, Lima BP, Wolfe AJ. Bacterial protein acetylation: the dawning of a new age. Mol. Microbiol. 2010; 77:15–21. [PubMed: 20487279]
9. Kim GW, Yang XJ. Comprehensive lysine acetylomes emerging from bacteria to humans. Trends Biochem. Sci. 2011; 36:211–220. [PubMed: 21075636]

10. Schwer B, Bunkenborg J, Verdin RO, Andersen JS, Verdin E. Reversible lysine acetylation controls the activity of the mitochondrial enzyme acetyl-CoA synthetase 2. Proc. Natl. Acad. Sci. USA. 2006; 103:10224–10229. [PubMed: 16788062]
11. Hirschey MD, Shimazu T, Huang JY, Schwer B, Verdin E. SIRT3 regulates mitochondrial protein acetylation and intermediary metabolism. Cold Spring Harb. Symp. Quant. Biol. 2011 Epub ahead of print.
12. Yu BJ, Kim JA, Moon JH, Ryu SE, Pan JG. The diversity of lysine-acetylated proteins in Escherichia coli. J. Microbiol. Biotechnol. 2008; 18:1529–1536. [PubMed: 18852508]
13. Wang Q, et al. Acetylation of metabolic enzymes coordinates carbon source utilization and metabolic flux. Science. 2010; 327:1004–1007. [PubMed: 20167787]
14. Zhang J, et al. Lysine acetylation is a highly abundant and evolutionarily conserved modification in Escherichia coli. Mol. Cell Proteomics. 2009; 8:215–225. [PubMed: 18723842]
15. Thao S, Escalante-Semerena JC. Control of protein function by reversible N^{ε}-lysine acetylation in bacteria. Curr. Opin. Microbiol. 2011; 14:200–204. [PubMed: 21239213]
16. Castano-Cerezo S, Bernal V, Blanco-Catala J, Iborra JL, Canovas M. cAMP-CRP co-ordinates the expression of the protein acetylation pathway with central metabolism in Escherichia coli. Mol. Microbiol. 2011; 82:1110–1128. [PubMed: 22059728]
17. Nanchen A, Schicker A, Revelles O, Sauer U. Cyclic AMP-dependent catabolite repression is the dominant control mechanism of metabolic fluxes under glucose limitation in Escherichia coli. J. Bacteriol. 2008; 190:2323–2330. [PubMed: 18223071]
18. Nambi S, Basu N, Visweswariah SS. cAMP-regulated protein lysine acetylases in mycobacteria. J. Biol. Chem. 2010; 285:24313–24323. [PubMed: 20507997]
19. Xu H, Hegde SS, Blanchard JS. Reversible acetylation and inactivation of Mycobacterium tuberculosis acetyl-CoA synthetase is dependent on cAMP. Biochemistry. 2011; 50:5883–5892. [PubMed: 21627103]
20. Nystrom T, Neidhardt FC. Expression and role of the universal stress protein, UspA, of Escherichia coli during growth arrest. Mol. Microbiol. 1994; 11:537–44. [PubMed: 8152377]
21. Crosby HA, Pelletier DA, Hurst GB, Escalante-Semerena JC. System-wide studies of N-Lysine acetylation in Rhodopseudomonas palustris reveals substrate specificity of protein acetyltransferases. J. Biol. Chem. 2012; 287:15590–15601. [PubMed: 22416131]
22. Vetting MW, et al. Structure and functions of the GNAT superfamily of acetyltransferases. Arch. Biochem. Biophys. 2005; 433:212–226. [PubMed: 15581578]
23. Fraser JS, et al. Accessing protein conformational ensembles using room-temperature X-ray crystallography. Proc. Natl. Acad. Sci. USA. 2011; 108:16247–16252. [PubMed: 21918110]
24. Lang PT, et al. Automated electron-density sampling reveals widespread conformational polymorphism in proteins. Protein Sci. 2010; 19:1420–1431. [PubMed: 20499387]
25. Garrity J, Gardner JG, Hawse W, Wolberger C, Escalante-Semerena JC. N-lysine propionylation controls the activity of propionyl-CoA synthetase. J. Biol. Chem. 2007; 282:30239–30245. [PubMed: 17684016]
26. Nambi S, Badireddy S, Visweswariah SS, Anand GS. Cyclic AMP-induced conformational changes in mycobacterial protein acetyltransferases. J. Biol. Chem. 2012; 287:18115–18129. [PubMed: 22447926]
27. Kornev AP, Taylor SS, Ten Eyck LF. A generalized allosteric mechanism for cis-regulated cyclic nucleotide binding domains. PLoS Comput. Biol. 2008; 4:e1000056. [PubMed: 18404204]
28. Popovych N, Tzeng SR, Tonelli M, Ebright RH, Kalodimos CG. Structural basis for cAMP-mediated allosteric control of the catabolite activator protein. Proc. Natl. Acad. Sci. USA. 2009; 106:6927–32. [PubMed: 19359484]
29. Passner JM, Schultz SC, Steitz TA. Modeling the cAMP-induced allosteric transition using the crystal structure of CAP-cAMP at 2.1 A resolution. J. Mol. Biol. 2000; 304:847–859. [PubMed: 11124031]
30. Sharma H, Yu S, Kong J, Wang J, Steitz TA. Structure of apo-CAP reveals that large conformational changes are necessary for DNA binding. Proc. Natl. Acad. Sci. USA. 2009; 106:16604–16609. [PubMed: 19805344]

31. Kim C, Xuong NH, Taylor SS. Crystal structure of a complex between the catalytic and regulatory (RIalpha) subunits of PKA. Science. 2005; 307:690–696. [PubMed: 15692043]
32. Berman HM, et al. The cAMP binding domain: an ancient signaling module. Proc. Natl. Acad. Sci. USA. 2005; 102:45–50. [PubMed: 15618393]
33. Shenoy AR, Visweswariah SS. New messages from old messengers: cAMP and mycobacteria. Trends Microbiol. 2006; 14:543–550. [PubMed: 17055275]
34. Bai G, Knapp GS, McDonough KA. Cyclic AMP signalling in mycobacteria: redirecting the conversation with a common currency. Cell Microbiol. 2011; 13:349–358. [PubMed: 21199259]
35. Munoz-Elias EJ, et al. Replication dynamics of Mycobacterium tuberculosis in chronically infected mice. Infect. Immun. 2005; 73:546–551. [PubMed: 15618194]
36. Gill WP, et al. A replication clock for Mycobacterium tuberculosis. Nat. Med. 2009; 15:211–214. [PubMed: 19182798]
37. Wayne LG. Synchronized replication of Mycobacterium tuberculosis. Infect. Immun. 1977; 17:528–530. [PubMed: 409675]
38. Brent MM, Iwata A, Carten J, Zhao K, Marmorstein R. Structure and biochemical characterization of protein acetyltransferase from Sulfolobus solfataricus. J. Biol. Chem. 2009; 284:19412–19419. [PubMed: 19473964]

References for Online Methods

39. Van Duyne GD, Standaert RF, Karplus PA, Schreiber SL, Clardy J. Atomic structures of the human immunophilin FKBP-12 complexes with FK506 and rapamycin. J. Mol. Biol. 1993; 229:105–124. [PubMed: 7678431]
40. Otwinowski, Z.; Minor, W. Processing of X-ray diffraction data collected in oscillation mode. In: Carter, Charles W., Jr., editor. Methods in Enzymology. Vol. 276. Academic Press; 1997. p. 307-326.
41. Leslie AGW. Recent changes to the MOSFLM package for processing film and image plate data. Joint CCP4 + ESF-EAMCB Newsletter on Protein Crystallography. 1992:26.
42. Collaborative Computational Project, N. The CCP4 Suite: Programs for Protein Crystallography. Acta Crystallographica. 1994; D50:760–763.
43. Adams PD, et al. PHENIX: a comprehensive Python-based system for macromolecular structure solution. Acta Crystallogr. D Biol. Crystallogr. 2010; 66:213–221. [PubMed: 20124702]
44. Langer G, Cohen SX, Lamzin VS, Perrakis A. Automated macromolecular model building for X-ray crystallography using ARP/wARP version 7. Nat. Protoc. 2008; 3:1171–1179. [PubMed: 18600222]
45. Emsley P, Cowtan K. Coot: model-building tools for molecular graphics. Acta Crystallogr. D Biol. Crystallogr. 2004; 60:2126–2132. [PubMed: 15572765]
46. McCoy AJ, et al. Phaser crystallographic software. J. Appl. Crystallogr. 2007; 40:658–674. [PubMed: 19461840]
47. Murshudov GN, et al. REFMAC5 for the refinement of macromolecular crystal structures. Acta Crystallogr. D Biol. Crystallogr. 2011; 67:355–367. [PubMed: 21460454]
48. Cowtan K. The Buccaneer software for automated model building. 1. Tracing protein chains. Acta Crystallogr. D Biol. Crystallogr. 2006; 62:1002–1011. [PubMed: 16929101]
49. Chen VB, et al. MolProbity: all-atom structure validation for macromolecular crystallography. Acta Crystallogr. D Biol. Crystallogr. 2010; 66:12–21.
50. Larkin MA, et al. Clustal W and Clustal X version 2.0. Bioinformatics. 2007; 23:2947–2948. [PubMed: 17846036]
51. Kabsch W, Sander C. Dictionary of protein secondary structure: pattern recognition of hydrogen-bonded and geometrical features. Biopolymers. 1983; 22:2577–2637. [PubMed: 6667333]
52. Pettersen EF, et al. UCSF Chimera--a visualization system for exploratory research and analysis. J Comput Chem. 2004; 25:1605–1612. [PubMed: 15264254]

53. Neuwald AF, Landsman D. GCN5-related histone N-acetyltransferases belong to a diverse superfamily that includes the yeast SPT10 protein. Trends Biochem. Sci. 1997; 22:154–155. [PubMed: 9175471]

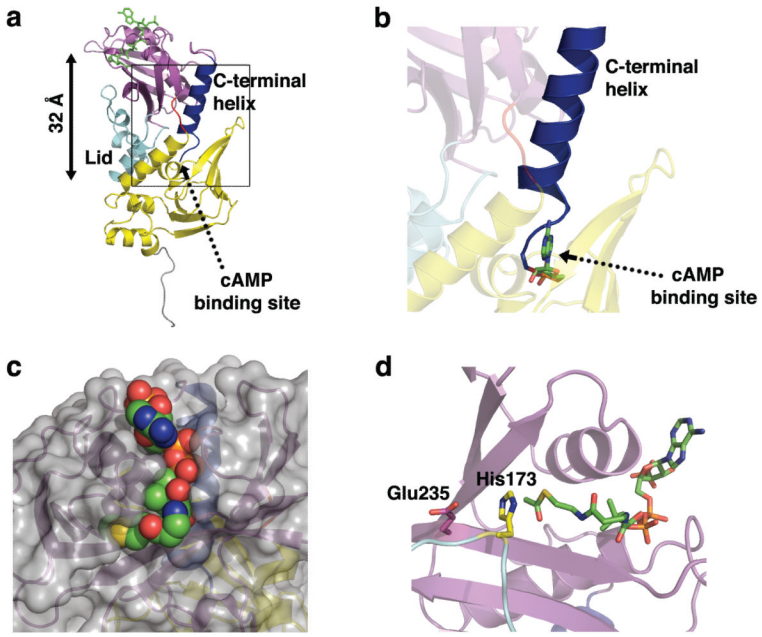

Figure 1. A double steric latch auto-inhibits Mt-PatA

(**a**) Overall fold of Mt-PatA. The N-terminal regulatory domain (yellow) is joined to the catalytic PAT domain (magenta) by a short extended linker (red). A lid (cyan) inserted in the PAT domain buries the catalytic site, and a helix appended to the C-terminus of the PAT domain extends back to the regulatory domain and fills the cAMP-binding site. The bound acetyl-CoA substrate (green) is shown in stick representation.

(**b**) The C-terminus occupies the cAMP-binding site in the regulatory domain. The surface of the cAMP-binding site (dashed arrow) engages the protein C-terminus. The terminal carboxylate of Gly333 and modeled cAMP are shown in stick representation. This figure is a view of the box in Fig. 1a.

(**c**) Acetyl-CoA (spheres) binds in a shallow groove formed by conserved motifs of the PAT domain [53].

(**d**) His173 (yellow) in the lid (cyan), contacts the catalytic base (Glu235, magenta), covers the acetyl donor and mimics a lysine substrate. Acetyl-CoA (green) and side chains are shown in stick model. The PAT domain is shown in magenta.

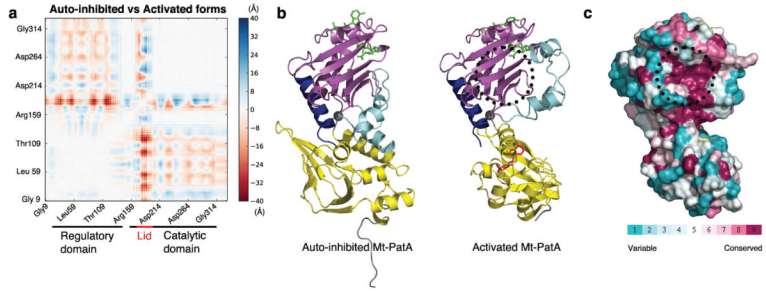

Figure 2. Crystal structure of the active form of Mt-PatA

(**a**) Difference-distance matrix between auto-inhibited and activated forms of Mt-PatA. Colors represent Cα differences of −40 to 40 Å.

(**b**) Ribbon diagram of the auto-inhibited (left) and cAMP-activated (right) forms of Mt-PatA. The regulatory (yellow) and catalytic domains (magenta) are dramatically reoriented, and the lid (cyan) refolds. The C-terminal helix (blue) remains packed against the PAT domain. The hinge in the interdomain linker, Ser144, is shown as a gray sphere. Bound Ac-CoA (green) and cAMP (red) molecules are shown as sticks.

(**c**) Sequence conservation displayed on the surface of the activated form of Mt-PatA shows that lid opening exposes a conserved surface (purple) around the acetyl donor site. Residues conserved in mycobacterial Mt-PatA orthologs include central β-strands of the catalytic domain and the residues binding the pantothenyl arm of acetyl-CoA. The view is the same as the activated form of Fig. 2b.

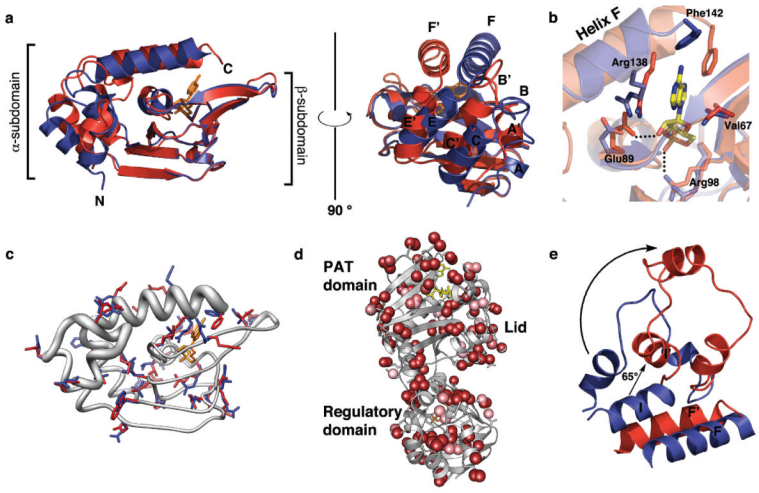

Figure 3. Mechanisms of interdomain communication

(**a**) Regulatory domains of auto-inhibited (blue) and active (red, ') states superimposed using residues 37-113 reveal large shifts in the helical subdomain stabilized by cAMP (orange).

(**b**) Cyclic-AMP binds at the N-terminus of a short helix and contacts conserved residues Glu89 and Arg98. Arg138 and Phe142 in helix F reorient to interact with the adenine ring.

(**c**) Rotamer flips mediate the large conformational change in the regulatory domain upon binding cAMP (orange). Superimposed side chains (sticks) with *Ringer* correlation coefficients <0.2 between the electron density maps of the auto-inhibited (blue) and active (red) structures illustrate the extensive conformational remodeling. The backbone thickness is proportional to the Cα difference.

(**d**) Residues on the active surface of Mt-PatA switch rotamers upon cAMP binding. Dihedral angles (balls) with *Ringer* correlation coefficients <0.2 (pink) or <0 (red) between the electron density maps of the active and auto-inhibited forms are displayed on the active form. Ac-CoA (yellow) marks the catalytic site. Over 37% of residues have *Ringer* correlation coefficients <0.2. Lid opening couples switches on the protein-substrate binding surface in the PAT domain (top) to changes in the regulatory domain (bottom).

(**e**) The lid refolds to avoid a steric clash with the regulatory domain. The rotation of the regulatory domain exposes the cAMP-binding site and opens the lid. Helix F interacts with the helix I of the lid in the auto-inhibited state (blue), but changes stabilized by cAMP eliminate contacts between these helices (') in the activated state (red).

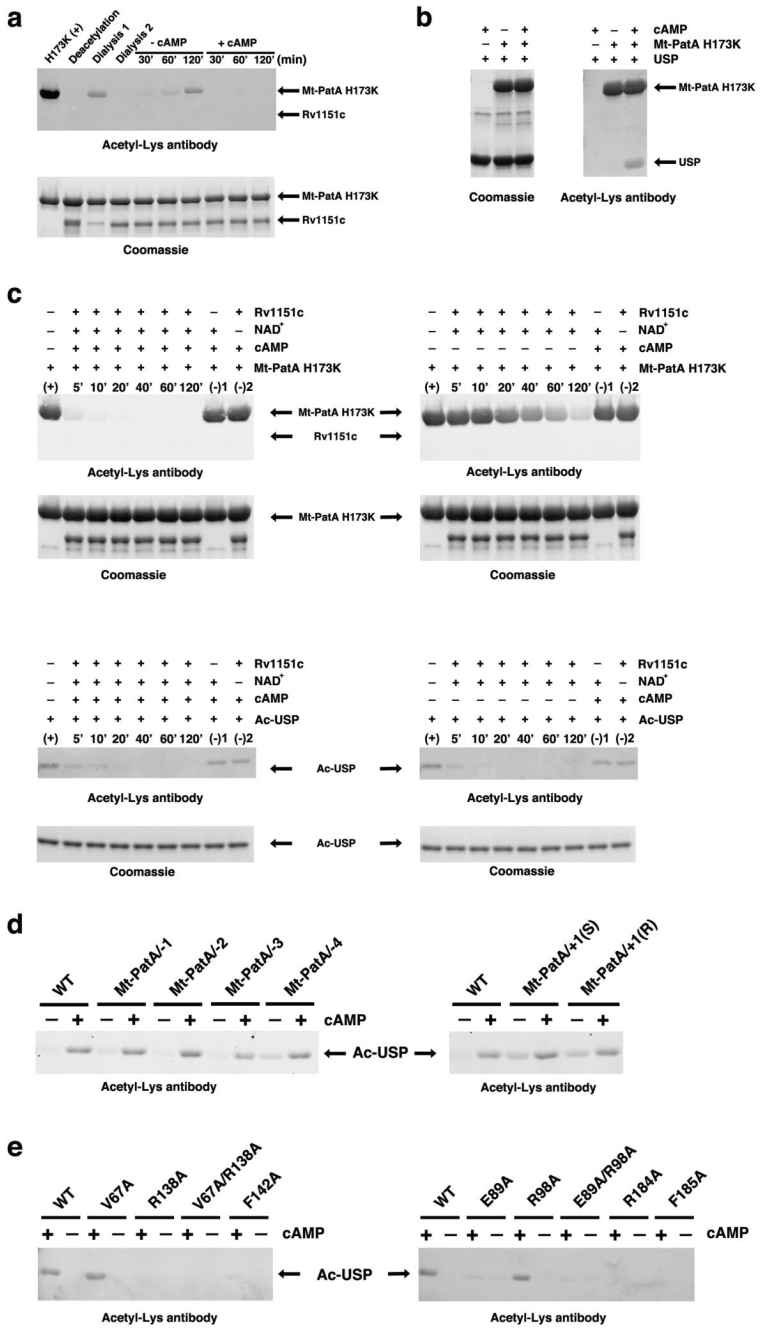

Figure 4. Mutants support a two-state model for Mt-PatA activation

(**a**) Auto-acetylation of His173Lys +/− cAMP. Purified His173Lys Mt-PatA (lane 1) was de-acetylated, dialyzed and de-acetylated again with Rv1151c (lanes 2-4). The His173Lys protein auto-acetylated efficiently in the absence but not presence of cAMP (lane 5-10). (**b**) Acetylation of USP by His173Lys +/− cAMP shows that cAMP activates the mutant enzyme to acetylate a heterologous substrate. USP alone (lane 1), or incubated with Mt-PatA His173Lys variant in the absence or presence of cAMP (lanes 2 and 3).

(**c**) Deacetylation of Ac-His173Lys +/− cAMP and Ac-USP by Rv1151c +/− cAMP. Cyclic-AMP indirectly stimulates deacetylation of the Mt-PatA His173Lys by stabilizing the open conformation, but has no effect on deacetylation of USP.
(**d**) Activity of C-terminal-truncations/additions. Deletion of four residues (-4) or addition of a Ser (+S) or Arg (+R) at the C-terminus activates Mt-PatA in the absence of cAMP. In contrast, Ala substitutions of conserved residues that contact cAMP block activation. These results emphasize the importance of the fit of the C-terminus into the regulatory site to form a “latch” that stabilizes the auto-inhibited state relative to the active state.
(**e**) Changes in activity of mutants in the cAMP-binding-site (≤ residue 142) and lid (Arg184 and Phe185) reveal sites important to activate the enzyme.

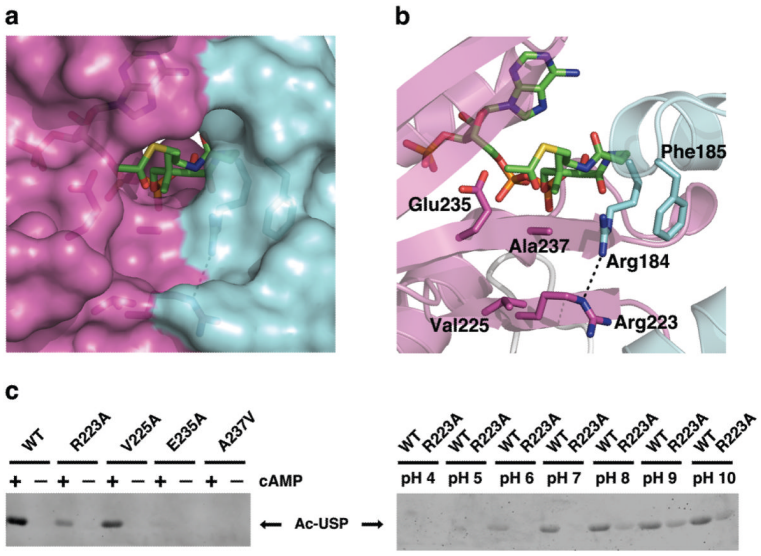

Figure 5. The open lid in the active state uncovers a cavity for the substrate Lys

(**a**) Surface representation of the active conformation shows the access tunnel for the substrate Lys. Residues in the lid (cyan) and the conserved catalytic domain (magenta) form the surface surrounding the tunnel. Ac-CoA (sticks) projects the acetyl group (green C) and the sulfur of the leaving group (gold) into the active site.

(**b**) Ribbon diagram of the binding surface for the substrate Lys in a same view and colors as Fig. 5a. The Arg184-Arg223 hydrogen bond is shown as a dotted line.

(**c**) Catalytic site mutants reveal residues important for acetyl transfer. The pH dependence of the activity of wild-type (activity at pH 8 ≥ pH 9) and Arg223Ala (activity at pH 9 > pH 8) variants suggest the importance of Arg223 in modulating the substrate Lys pK_a.

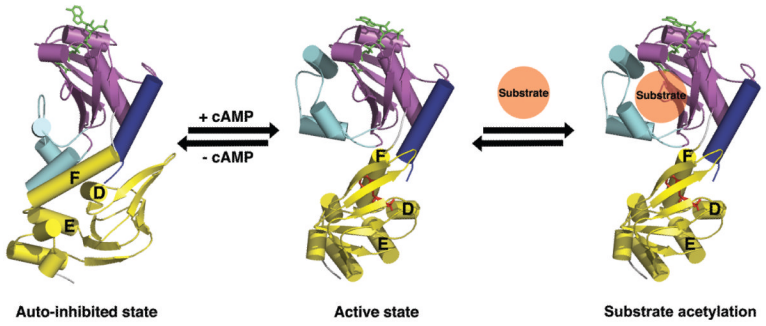

Figure 6. A steric double-latch regulates Mt-PatA

Release of the steric double-latch stabilized by cAMP binding. The N-terminal regulatory domain and the catalytic PAT domain are shown in yellow and magenta, respectively. The lid is shown in cyan, and the C-terminal helix is shown in blue. Cooperative interdomain communication is achieved indirectly, because the changes the regulatory domain stabilized by cAMP are incompatible with the closed lid.

Table 1

Data collection, phasing and refinement statistics

	Mt-PatA:Ac-CoA (Native)	Mt-PatA:Ac-CoA (SeMet)		Mt-PatA:Ac-CoA:cAMP (Native)	Mt-PatA:Ac-CoA:cAMP (SeMet)	
Data collection						
Space group	$P2_12_12_1$	$P2_12_12_1$		P1	$P2_1$	
Cell dimensions						
a, *b*, *c* (Å)	61.42, 65.45, 77.77	60.96, 65.18, 77.63	60.78, 64.92, 77.35	50.73, 60.12, 68.24	68.66, 50.15, 110.10	68.70, 50.16, 110.20
α, β, γ (°)	90, 90, 90	90, 90, 90	90, 90, 90	90.8, 111.7, 114.3	90, 106.6, 90	90, 106.6, 90
		Peak	*Remote*		*Peak*	*Remote*
Wavelength (Å)	1.1159	0.9796	0.9720	1.1159	0.9796	0.9569
Resolution (Å)	45-1.70	78-2.30	50-2.1	44-1.8	40-2.80	40-2.80
	(1.73-1.70)[a]	(2.36-2.30)	(2.13-2.08)	(1.90-1.80)	(2.85-2.80)	(2.85-2.80)
R_{sym} or R_{merge}	0.071(0.754)	0.083 (0.331)	0.097 (0.622)	0.071 (0.27)	0.106 (0.399)	0.094 (0.454)
$I / \sigma I$	30 (1.6)	9.1 (3.1)	9.9 (2.2)	9.7 (3.2)	11 (1.91)	10.8 (1.8)
Completeness (%)	98.4 (99.7)	98.9 (98.9)	99.5 (99.3)	83.5 (87.6)	98.5 (97.5)	98.6 (98.0)
Redundancy	3.9 (3.8)	3.6 (3.7)	3.9 (3.9)	2.9 (2.8)	2.2 (2.3)	2.2 (2.3)
Refinement						
Resolution (Å)	44.79–1.70 (1.74–1.70)			32.12–1.8 (1.83–1.8)	39.88–2.80 (2.98–2.80)	
No. reflections	34,696			50,544	16,793	
R_{work} / R_{free}	0.1908/0.2296			0.174/0.216	0.1985/0.2672	
No. atoms						
Protein	2,493			4,915	4,925	
Ligand/ion	86			217		
Water	242			492	83	
B-factors						
Protein	38.10			23.87	39.03	
Ligand/ion	35.89			29.39	43.17	
Water	42.82			32.65	23.23	
R.m.s deviations						

Nat Struct Mol Biol. Author manuscript; available in PMC 2013 February 01.

	Mt-PatA:Ac-CoA (Native)	Mt-PatA:Ac-CoA (SeMet)	Mt-PatA:Ac-CoA:cAMP (Native)	Mt-PatA:Ac-CoA:cAMP (SeMet)
Bond lengths (Å)	0.010		0.005	0.012
Bond angles (°)	1.411		1.089	1.213

[a]Values in parentheses are for highest-resolution shell. The data were collected from one crystal.